LABORATORY TECHNIQUES

Conductivity Sensors Based System Development and Application to Investigate the Interfacial Behaviour between Supersonic Steam Jet and Water

Afrasyab Khan[a,*], Khairuddin Sanaullah[b], E. K. Spiridonov[a], A. V. Podzerko[a], D. F. Khabarova[a], Ahmad Hasan Ali[a], Ahmad Salam Farooqi[c,d], Mohammed Zwawi[e], Mohammed Algarni[e], Bassem F. Felemban[f], Ali Bahadar[g], Atta Ullah[h], and Bawadi Abdullah[i,j]

[a] *Polytechnic Institute of South Ural State University (National Research University),*
Chelyabinsk, 454080 Russia

[b] *Department for Management of Science and Technology Development, Faculty of Applied Sciences, Ton DucThang University,*
Ho Chi Minh City, Vietnam

[c] *Department of Chemical Engineering, University Technology Petronas, Bandar Seri Iskandar,*
Perak, 32610 Malaysia

[d] *Department of Chemical Engineering, Wah Engineering College, University of Wah, WahCantt,*
Punjab, 47040 Pakistan

[e] *Department of Mechanical Engineering, King Abdulaziz University,*
Rabigh, 21911 Saudi Arabia

[f] *Mechanical Engineering Department, Taif University,*
Taif, 26571 Saudi Arabia

[g] *Department of Chemical and Materials Engineering, King Abdulaziz University,*
Rabigh, 21911 Saudi Arabia

[h] *Department of Chemical Engineering, Pakistan Institute of Engineering and Applied Sciences (PIEAS),*
Nilor, Islamabad, Pakistan

[i] *Chemical Engineering Department, Universiti Teknologi PETRONAS, Seri Iskandar, 32610 Malaysia*

[j] *CCentre of Contaminant Control and Utilization (CenCoU), Institute of Contaminant Management for Oil and Gas,*
Universiti Teknologi PETRONAS, Seri Iskandar, 32610 Malaysia
*e-mail: khana@susu.ru; drafrasyabkhan7@gmail.com
Received December 3, 2020; revised March 11, 2021; accepted March 15, 2021

Abstract—This study is an effort to comprehend the description of the vapour-liquid flows associated with the transformation of the phase, which may assist in determining mass, momentum and energy transfer within the interfacial region containing the steam and water. This study describes the development of a void fraction measurement sensory system, which is based on AC based electrodes, referred scientifically as Electrical Resistance Tomography (ERT) system. ERT sensors based system was applied to emphasize the phenomenon involving supersonic steam injection into a column of water. Data acquisition system supporting the ERT technique was applied for the given time interval and the acquired data was processed by using a free code known as EIDORS. Images thus obtained by use of EIDORS provided a planar picture of supersonic steam jet surrounding by the water in a vessel. Images represent the broadly visible boundaries among steam and water phases, and the turbulent interface between them. It has been found that with rising temperature 30–60°C, the area under the effect of the steam jet has been increased from 46.51–65.40% at 3.0 bar of steam's inlet pressure.

1. INTRODUCTION

The direct contact condensation (DCC) involving steam and water is applicable in a range of industries, including nuclear and thermal power plants and several process and metallurgical industries. The major benefit of DCC is due to the superior heat transfer across the vapor−liquid interface [1]. After the steam's injection into a vessel filled with sub-cooled water, condensation of steam occurs, which, depending on the operating conditions, may adopt three flow regimes; bubbling, chugging and jet [2].

The DCC remains an issue of interest as manifested in previous studies that includes many like e.g. Kerney et al. [3] and Weimer et al. [4]. They per-
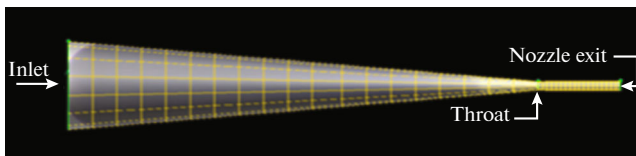
Fig. 1. A schematic of a supersonic nozzle.

formed experiments and reported the normalized penetration of the steam jet, which was validated theoretically. However, they studied the influence of water temperature on the dimensions of the interfacial region among steam and water.

Their results indicated the geometry of the interfacial zone that largely depended on the temperature. Theoretical model has been applied [5] to explain the condensation phenomena, which included the description upon the distribution of pressure and temperature within the steam's plume and its surroundings. Most of the work accomplished till the date has been mainly focused on the flow regimes that prevail within the body of the steam's plume/jet, and its neighbourhood, as well as on the modes of heat and mass transfer.

However, there was no study that reported detailed spatial temperature distribution to show the origin of the hydrodynamic instabilities across the steam's jet and its interaction with the water as its surrounding fluid. Few of our studies has shed light on it [6–8], but still the interfacial behavior and its trends need to be examined by the use of more sophisticated techniques like the ERT as described here.

The interaction between the steam and water is characterized due to the formation of interface between the two phases. The nature of the interface is very unstable, also, the transfer of mass, momentum and energy depends on the nature of interface and these occur through the interface between them. Capturing the characteristics of the interface by experimental, theoretical, and/or computational ways is complicated because of its unstable nature. Also, mass, momentum and heat transfer across the transiently varying interface makes this phenomena more complex.

As described before, more intensive research on the steam-water interfacial phenomenon is significant due to the generation of Kelvin−Helmholtz (KH) instabilities [6] and the interfacial steam's condensation at large-scale leading to water knocking in the piping of a nuclear power plant [9], which may leave an adverse effect towards the safety and integrity of the installations. The KH instabilities are responsible to destabilizing the interface among the steam and water in DCC [10]. They sustain for short time period and are damped due to the temperature and viscosity of the water surrounding the steam's jet [7, 11].

Such instabilities form at the interface and they propagate further from the interface, towards the out side direction. The interface between the steam and water has been assumed having a nil thickness [9]. Others, [12−16], who contributed significant information on interfacial instabilities of condensable and non-condensable fluids, emphasized over the need of having precise information in the column, where the multiphase flow occurs and a single most significant variable that controls the phenomena across the interface is the void fraction. Thus, any error in the measured value of void fraction may lead to wrong convictions about the understanding of the interfacial phenomena. This may result into erroneous results for the heat, mass, and momentum transport across the interface.

We are aware that for the accurate measurements, we must only have to rely on the non-invasive techniques, that do not disturb the flow due to their physical intrusion inside the flow domain. Also, the development of invasive fluid measurement setups and their maintenance is indeed expensive. In spite of the significance of the void fraction in affecting the other important parameters that govern the overall interfacial flow between the interacting gas and liquid, it also relies on many variables, including gas pressure, thermodynamics, geometry and dimensions of the vessel, flow rates of liquid and gas, etc.

The current investigation concentrates on the characterization of the interfacial phenomena by means of the application of ERT technique to obtain non-invasive scans including the areas under the effect of the body of steam's jet as well as surrounding water. In order to quantify the impact of the surrounding conditions (i.e., the temperature of the surrounding water), we attempted here to determine the void fraction of supersonic steam jet in water from the ERT scans. These scans were based on the difference in the electrical conductivities between the gaseous and liquid phases. Also, it has been made every effort to maintain the temperature of the subcooled water uniform within the vessel, or at least during time interval when the ERT device was in use to secure the fluid's scan in the vessel at the elevation of the electrodes mounted on the inner walls of the vessel.

ERT is a useful technique to characterize the fluid phase in process vessels containing multiphase flows by recording the gradient in the conductivities [17]. However, the suitability of the method for multiphase flow diagnostics has been related to those instances, wherever the continuous phase is conductive along with existence of the gradient of conductivity across the interacting fluid layers of different phases. In those situations, when the continuous phase is the liquid and gas/vapor as the dispersed medium, ERT can be used under such cases to measure the void fraction [18]. However, the usefulness of the method is challenged in measuring the phase distributions and phasic
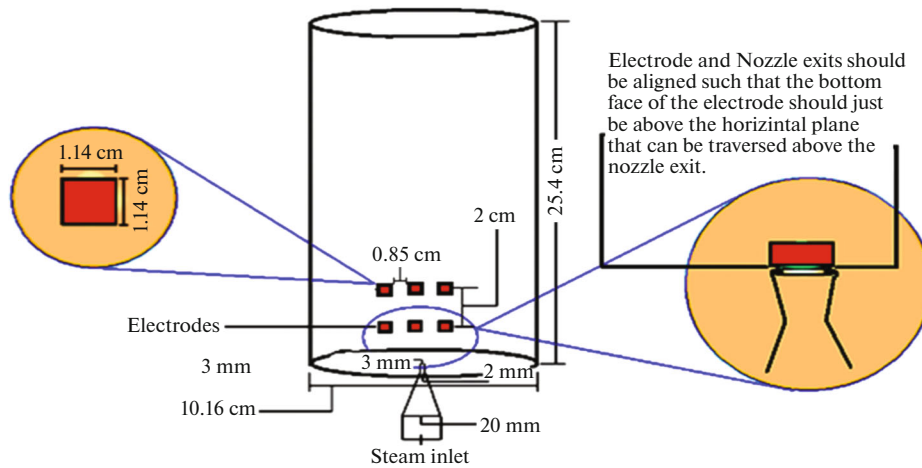
Fig. 2. A schematic of vessel and layout of mounted electrodes.

velocities that may vary substantially both on temporal and spatial basis [19]. Thus, for flow diagnostic measurements, the key requirements are the equipment's accuracy as well as it should not disturb the fluid flow due to intrusion. However, such requirements can never be achieved due to the physical size/shape of the sensors, if they have to intrude inside the body of the fluids. So, to determine the conductivity and its variation across the flow domain correctly, the intrusion of the instrument inside the bodies of the interacting phases needs to be removed. This has led to the innovation of the fluid diagnostic technique that can capture change in electrical conductivity across the flow region of interacting fluids with the help of the electrodes being located on the circumferential wall of the vessel. This concept has steered towards accomplishing the task for the voidage measurements of multi phases in nuclear and process industries [20], petroleum [21] and many other applications.

The main aim of the current study is to alter the focus of the earlier investigations on the supersonic steam jet in water, with a more specific approach through the use of the conductivity scans from ERT.

2. EXPERIMENTAL SETUP

A specially configured nozzle having converging and diverging sections as shown in Fig. 1, was used to generate the supersonic steam's jet at operating gauge pressure gradient of 1.5−3.0 bar of gauge pressure.

The nozzle has been designed and validated for the generation of supersonic steam jet [6, 7]. Also, the capacity of the nozzle was successfully assessed using the CFD scheme corresponding to the gauge pressure
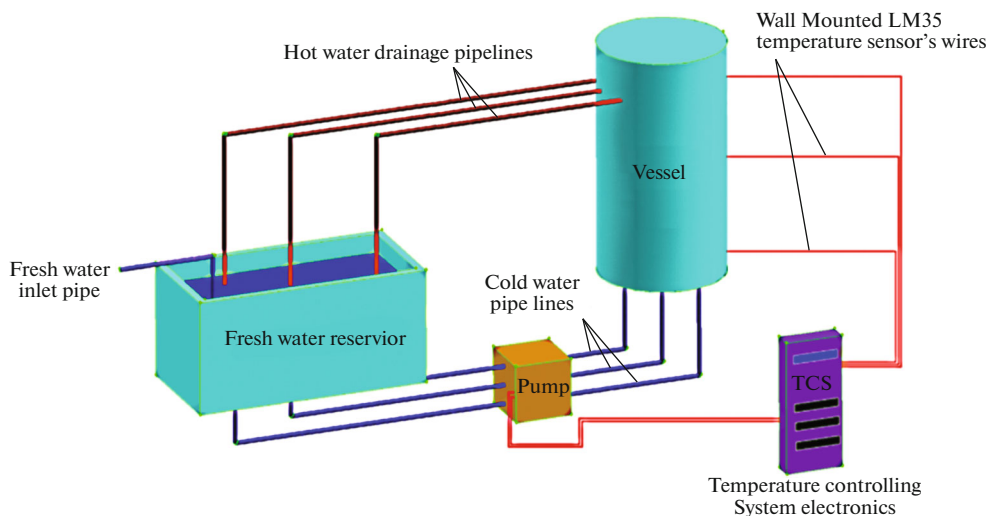

Fig. 3. Fresh water injection system.

Table 1. Operating conditions during experimentations

Serial no:	Quantity	Range	Increment	No. of data sets
1	Pressure, bar	1.5—3.0	0.5	4
2	Temperature of surrounding water (used in calibration as well as experimentation), °C	30—60	5	7
3	Nozzle inlet, mm	20	—	—
4	Nozzle throat, mm	2	—	—
5	Nozzle exit, mm	3	—	—
6	Diameter of the Teflon rod, mm	6.0	—	1
7	Temperature at which the Teflon rod has been heated in oven, °C	133.54; 127.41; 120.23; 111.37	—	4
8	Total calibration tests for each combination of diameter and temperature of Teflon rod	—	—	5
9	Total no. of calibration tests	—	—	140

of 1.5—3.0 bar through computations of DCC model [10]. The supersonic nozzle being part of the experimental setup, was connected to the boiler by the flexible teflon tube having spiral steel rings wrapped around it. The boiler could provide steam at maximum dynamic steam pressure of 4 bar. The schematic of column with layout of mounted electrodes can be seen in Fig. 2. Four rings of electrodes were flushed with the inner walls of the column with vertical separation between any of the two rings of electrodes was 2 cm. Also, the circumferential distance along the periphery of the column, between the centers of any two neighbouring electrodes was 0.85 cm. The bottom edge of the electrodes belonging to the bottom ring was just below the nozzle exit. It is useful to state here that steam's injection into the water through the nozzle follows the theory on compressible flow [22], which is based on the pressure gradient amongst the nozzle exit and the back pressure, leading to the generation of expansion waves at the nozzle's exit. As a result of a rise in the steam's pressure, a proportional influence has been exerted on the flow rate through the nozzle and the pressure at the nozzle's exit.

Thus, the region enclosing the nozzle's exit and its surrounding has significance in capturing the variation in conductivities by application of electrical potentials through these electrodes. Here, the mentioned scans belong to the most swollen part of the steam jet which is visually located at ~2.4—2.6 cm above the nozzle exit. Steam has been injected through the centre of the column. Thus, following the opposite electrodes arrangement along with fully "Flexible Sensing Strategy" scheme (FSS) [23] was used to capture the varying trends in the conductivities across the plane of our interest [24]. We selected to apply the potential across the electrodes in opposite electrode strategy, and the reason was that the steam jet was located at the center of the column. Other potential applying strategies includes the adjacent arrangement that provides higher sensitivity, however, this is applicable to the region adjacent to the walls of the column. The sizes of the electrodes were chosen by trusting the fact that the percentage of the surface exposed to the 16 electrodes should be 60% of the total surface of the region of interest to determine the highest distinguishability in the case of opposite arrangement [25].
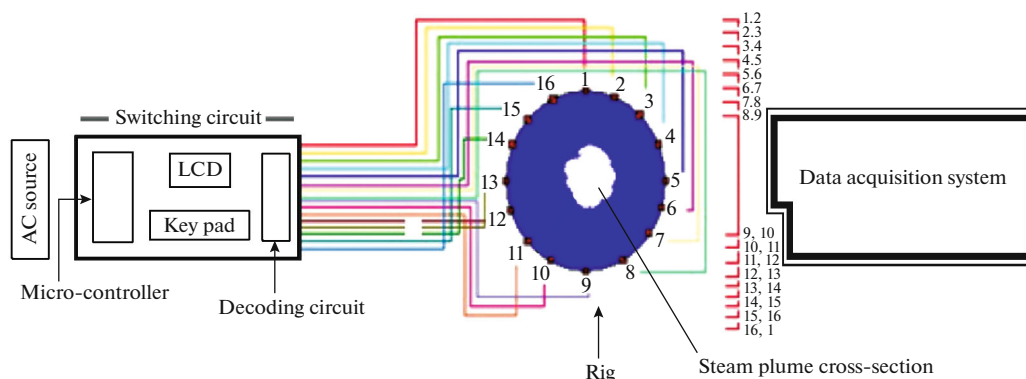

Fig. 4. A schematic layout of the sensor to characterise steam-water flow.

**Table 2.** Actual + over estimated void fractions using developed ERT system

Temperature of Teflon rod, °C	Corresponding pressure from steam data tables [28], bar	Total void fraction {actual + over-estimated} of Teflon rod, %							Actual void fraction of the Teflon rod, %
		Surrounding water temperature, °C							
		30	35	40	45	50	55	60	
133.54	3.0	81.02	81.32	82.08	82.24	82.83	82.99	83.44	0.35
127.41	2.5	72.14	75.21	75.39	79.21	79.46	79.85	79.83	0.35
120.23	2.0	54.91	54.91	65.41	65.41	65.46	69.49	71.08	0.35
111.37	1.5	46.16	46.16	46.16	46.16	46.63	50.31	50.59	0.35

Table 3. Calculated void fractions as mentioned in Fig. 11

Serial bo.	Steam inlet pressure, bar	Surrounding water temperature, °C	Fig. 11	Void fraction, %
1	3.0	30	11a	46.51
2	3.0	35	11b	46.62
3	3.0	40	11c	50.30
4	3.0	45	11d	50.93
5	3.0	50	11e	54.90
6	3.0	55	11f	62.31
7	3.0	60	11g	65.40

Moreover, the value of excitation current that was applied as 75 mA, whereas, the temperature of the water in the column was kept same (for the time duration when the ERT system was scanning the fluid medium). The temperature of the water has been kept constant for the time duration by maintaining a constant circulation of fresh water into the column as shown in Fig. 3. The fresh water was added from the base of the column in horizontal direction with the use of a pump being controlled by the temperature controlling system (TCS).

The development of sensor involving micro controller (AT89C51), key encoders (MM74C922), key decoders (74HC137) and solid state switches (Max 4665), was accomplished to determine the KH instabilities across the supersonic steam jet interacting interfacially with the surrounding water. 16 SS electrodes were fitted circumferentially around the column of 101.6 mm dia and this arrangement was positioned at 3 locations with a gap of 2 cm between each of the two electrode rings. 48 electrodes in total were thus used to develop the complete setup for the sensory system, which could record the variation in the
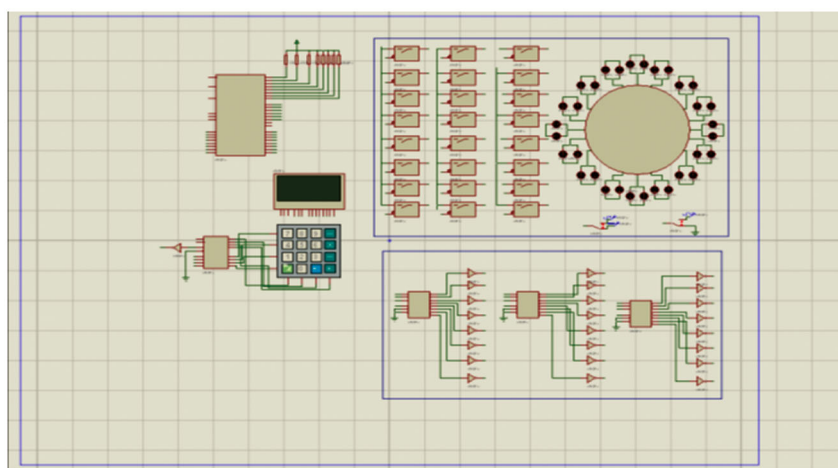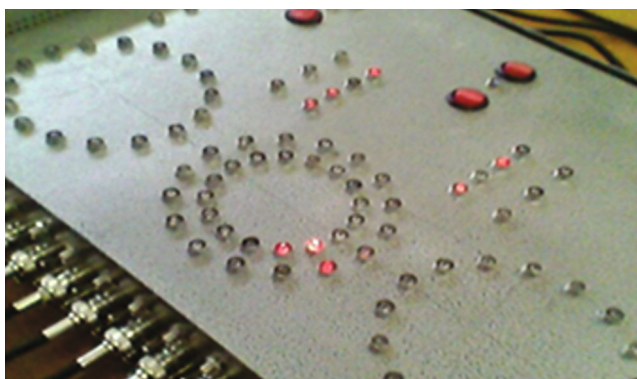

Fig. 5. Multiplexing circuit diagram.

Fig. 6. A snap showing multiplexing box.

size of the area and hence the interface occupied by the supersonic steam jet and water. The schematic of the sensor's electronic block arrangement can be seen in Fig. 4, whereas the plane of the electrodes mounted at the inner walls on the column can be seen in Fig. 2.

The sensor was operated by applying AC source that provided the 220 V at 50 Hz. Also, a battery having 5 V was used to drive DC supply to the micro-controller, whereas, the second battery with ± 12 V potential, was used to drive the solid state switches Max 4665. The power rating of the instrument was 3 mA while operating at maximum load. The micro controller with 8 bits had 4 ports, $0 \rightarrow 3$, which was used to derive input and apply control logic schemes: opposite, adjacent, and cosine. Figure 5 shows the circuit layout, whereas, the multiplex box is seen in the Fig. 6 that indicates that the adjacent signals being delivered to the adjoining electrodes as proved by same time blinking of 2 LEDs. It should be noted that we used all the three current injection strategies, i.e., the adjacent, opposite and cosine, but mentioned here the opposite strategy based scans as shown in figures afterwards. Hex keypad was connected to the port 3 of micro-controller through MM74C922 key encoder which was assigned to provide inputs to the system.

Whereas, HD 47780 and 16 × 4 LCDs were connected to the micro-controller through port 1, and 74HC137 decoders were assigned to port 2 to execute direct signal switching by adopting decoding schemes. Low resistance (5 Ω) analog switches, CMOS were used to drive the AC signals through the decoder 74HC137 to the electrodes. C language was applied using Keil IDE to develop a software for the sensor and the sequence of operations of the control program can be seen in Fig. 7 as a flow chart. AC signals have been applied onto the electrodes through the National Instruments Data Acquisition Card labeled as PCI-6033E, containing DAQ procedure. The electronic system containing 64 channels along with the banana switches, facilitated signal about each electrode, thus acquiring the data at 1000 samples in a second.
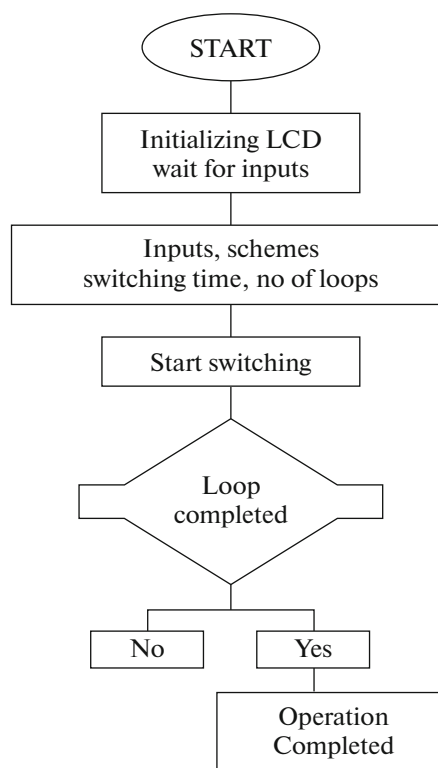

Fig. 7. A flow diagram showing the sequence of control program.

A neighbourhood scheme was adopted to link the banana switches with the electrodes. Electrodes 1 and 2 were linked with 2 banana switches through a single BNC1 cable, whereas, electrodes 2 and 3 were connected to the switches through BNC2 cable, as seen in Fig. 8. The scheme, thus, has been followed for all the 16 electrodes.

The raw data thus obtained, was filtered by applying the MATLAB's built in ML-FILTER. From two data sets, one was collected with no steam's injection, labeled as water file and the other was collected with steam's injection and this was referred as steam file. The profiles thus plotted from these data sets can be seen in Fig. 9, which represents a typical plot for 20 ms and similarly plots for 40, 60, 80, 100, 200, 400, 600, 800, and 1000 ms were acquired. The data for V_{rms} values was processed by corresponding to the range of
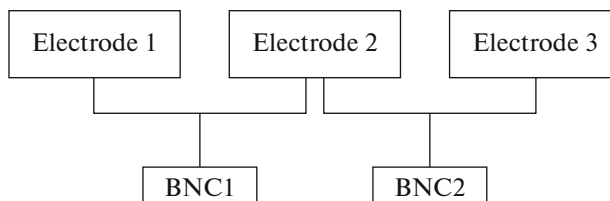

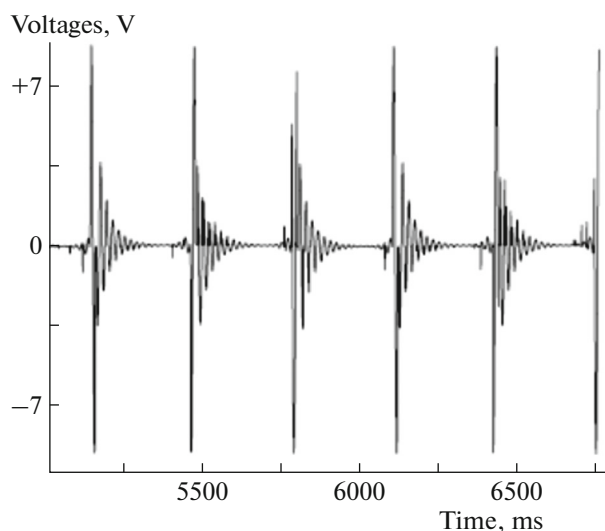**Fig. 8.** A layout of link between Banana switches and electrodes.

Fig. 9. A typical plot of steam data collected at 20 ms.

water temperature from 30 to 60°C, with an increment of 5°C, including all the time intervals. The acquired data was then processed with EIDORS to acquire the scan images reconstructed by following a finite element scheme representing forward computations and a normalized non-linear solver to acquire a unique and stable inverse solution [26]. EIDORS version 3.7.1 toolkit was used to process the data of the present experiments.

Calibration of the setup. The use of the ERT setup as a non-invasive fluid diagnostic technique has been proved in previous studies Electrical resistance tomographic sensing systems for industrial applications (Chem. Eng. Commun., 1999, vol. 175, pp. 49−70). The changes that brought in the conductivity of water governed by multiple factors that includes the concentration of the charge carriers, and the variations in the temperature of the water. It is, therefore the calibration of our developed system is inevitable for the proper information gathering related to the void frac-

tion measurements. For it we have used a Polytetra-flouroethlene (Teflon) rod with the same diameter ~6 mm as the supersonic steam jet has at the given pressure ~3 bar. The operating conditions with respect to the calibration tests have been given in the Table 1. The Teflon rod has been heated in an oven to a temperature that ranges from 111.37 to 133.54°C and it should be noted that the mentioned temperature range corresponds to a steam pressure of 1.5−3.0 bar. The heated rod has been dropped into the water in a vessel that has been connected to the designed and developed ERT system. As the electric resistance tomography (ERT) systems can only present the qualitative measurements for the phase distribution in terms of the conductivity of the fluid medium, so in order to assess its measurement capability on quantitative basis, these calibration tests are necessarily to be performed at the same hydrodynamic conditions, which we have used for the experimentation phase. The approximate dimensions of the Teflon rod, i.e., its diameter has been inferred from our previous studies [6, 27] conducted under the same conditions.

The same hydrodynamic conditions have been used in the calibration tests for mockup experimentation for supersonic steam jet injection into subcooled water. The steam data table [28] is used for getting the inference regarding the temperature which the supersonic steam jet could have at the inlet pressure ranging from 1.5−3.0 bar, i.e., 111.37−133.54°C respectively. The results of the calibration tests have shown that an over-estimation exists in the measurements obtained by developed ERT system. From the series of these calibration tests an over-estimation has been observed in the total void fraction (%). The measured void fraction (%) corresponds to the total volume of the Teflon rod (i.e., over-estimated void fraction + actual void fraction inside the slice of the fluid scanned by the single ERT ring of electrodes). It has been found that approximately ~45% over estimation exits at the surrounding water temperature of 30°C. when the rod has been heated to 111.37°C corresponding to 1.5 bar. The
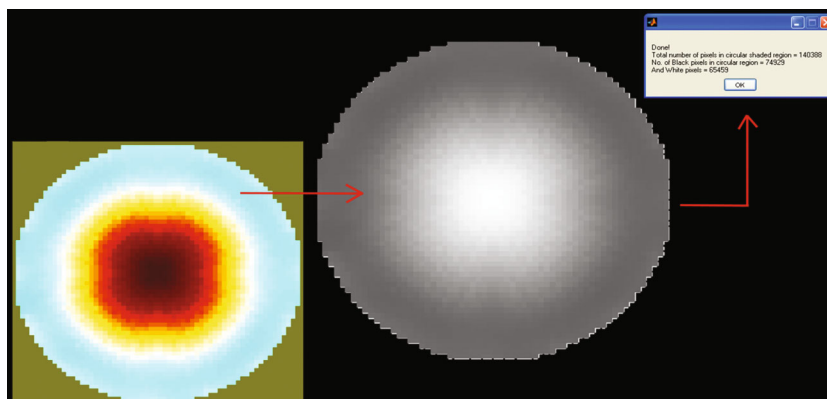

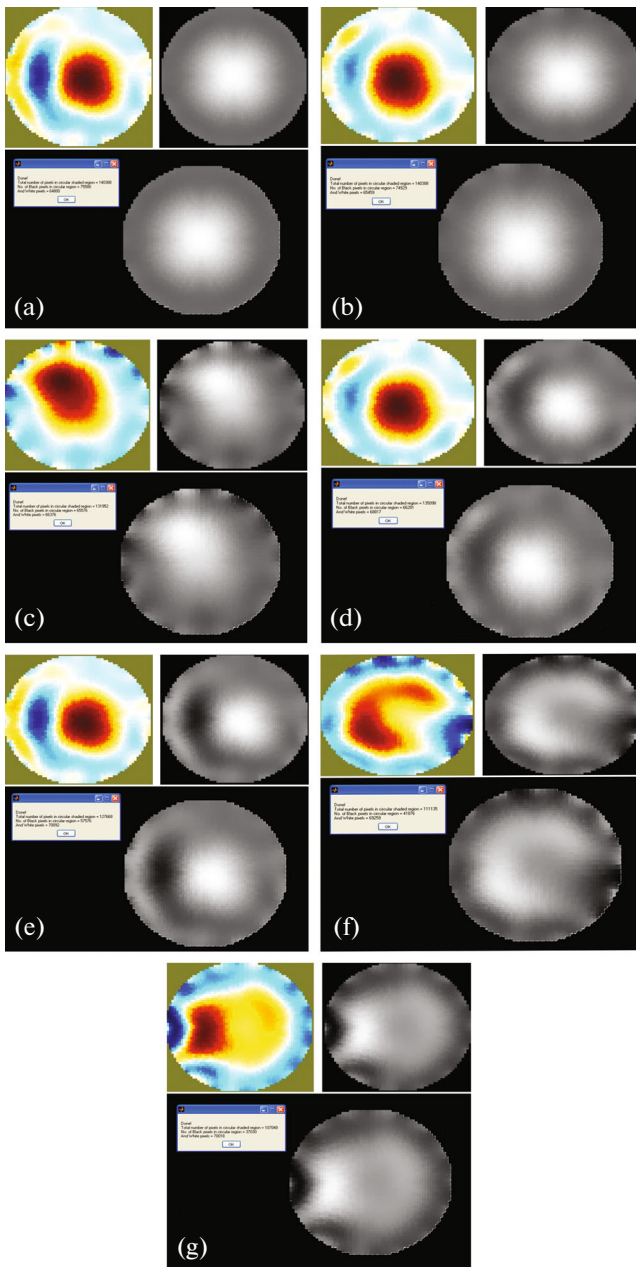**Fig. 10.** Conversion of the RGB image to grey scale image and no. of pixels.

Fig. 11. The boundaries of the "steam–water" section obtained with ERT, EIDORS and Matlab®, at a steam pressure of 3.0 bar and at various water temperatures from 30 to 60°C: (a) total volumetric steam content 46.51%, ambient water temperature 30°C; (b) 46.62%, 35°C; (c) 50.30%, 40°C; (d) 50.93%, 45°C; (e) 54.90%, 50°C; (f) 62.31%, 55°C; (g) 65.40%, 60°C.

Fig. 12. Qualitative steam void fractions as observed at different temperatures of water in the vessel.

3. RESULTS AND DISCUSSION

The data from ERT setup was treated with EIDORS to obtain the images, which are illustrated on the left at the bottom of Fig. 10.

This provided much improved views, which were converted into the grey scale images. Images has been then processed by using the Matlab® based "imread" function [29] to compute the sum of white and black pixels on grey scale images. Figure 11 shows tomographs of steam–water interface at varying sub cooling

over-estimation goes up to nearly ~83%, when the surrounding water temperature has been raised to 60°C and the rod is heated at 133.54°C that corresponds to 3.0 bar of steam pressure. The results comprised on the findings of a series of calibration tests and those reported here, are in fact the most repeating value with a confidence interval of more than 90%. The results of the calibration tests are shown in the Table 2.
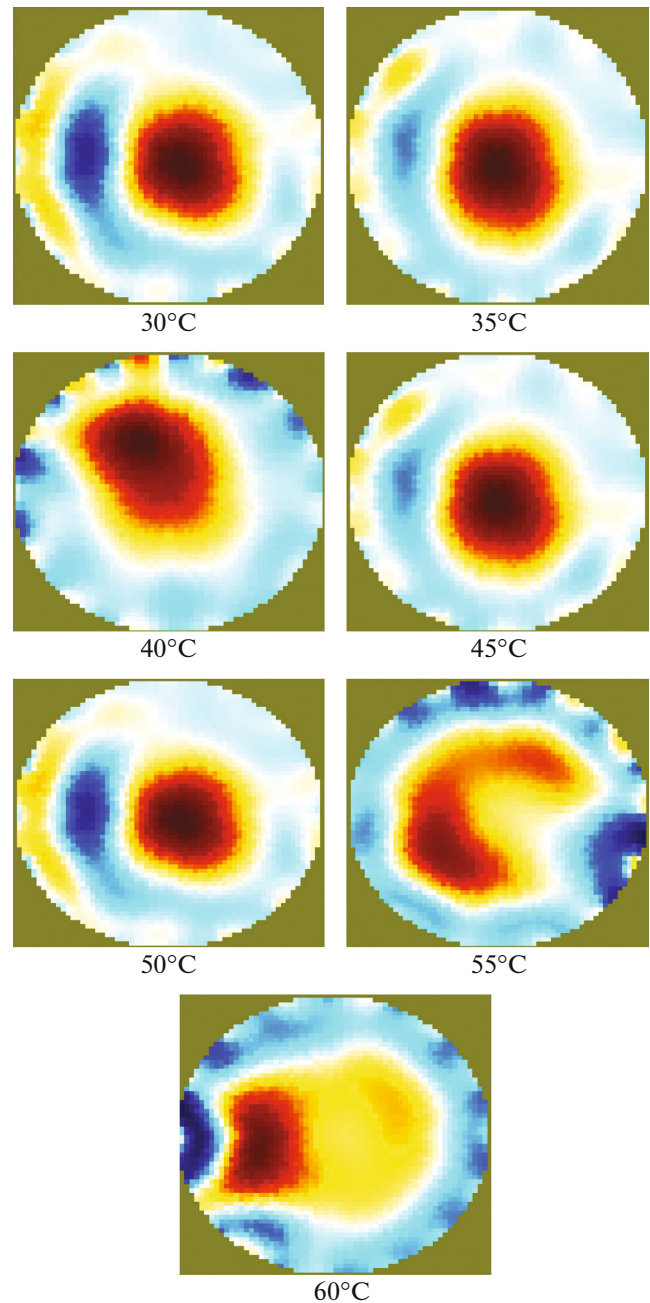
water temperatures from 30 to 60°C at fixed steam pressure of 3 bar, which were obtained by employing ERT setup and EIDORS, along with image processing techniques in Matlab®. It has been evident from these scans that no considerable change apart from minor fluctuations associated to the steam's jet was noticed in total void fraction due to the supersonic steam's jet against the representative operating conditions. From these scans, the total void fraction (i.e., overestimated + real) of the supersonic steam jet at steam pressure, 3.0 bar (yet we acquired scan images at varying pressure from 1.5–3.0 bar, but here for the sack of more clear scans, we mentioned the scans at 3.0 bars only), and temperature of the surrounding water, 30–60°C, has been acquired as given in Table 3.

From this table, it can obviously be noted of the change in the approximate void fraction due to the change in the temperature of the surrounding water. Thus, with the rise in the temperature of the surrounding water, the interface and the area occupied by the steam jet and its surrounding interface has been raised. At lower temperature of the surrounding water (i.e., 30–35°C) the change in the void fractions (i.e., 46.51–46.62%) is not so much obvious, which slowly rises with the rise in the surrounding water temperature up till 60°C. The main reason for the rise in this area under the influence of the steam itself and its interface could be the enhanced heat transfer across the interface of the steam with the surrounding water. The transfer of the heat from the steam jet to the surrounding water may be enhanced as at the higher temperature of the surrounding water, the hydrodynamic instabilities become dominant at the interface due to the lower dense water being in contact with the steam interface at that time [6].

Other information that was relied on change in conductivity through supersonic steam jet scans was obtained to estimate the propogation of the hydrodynamic instabilities induced temperature variation as shown in the Fig. 12. As it can be seen that at the higher elevated temperature i.e., 55–60°C, the temperature variation has been recorded uptill the walls of the water column.

The uneven distribution of the conductivities as being evident in the tomographic scans, reveal the characteristic regions owing to the steam's jet, the water region, and the interfacial area. However, the fluctuating nature of the steam jet indicates the rough structure of the jet along with supports towards the fluctuating behaviour of the steam–water interface. It was found that the steam–water interface not only produceed hydrodynamic instabilities as shown by the uneven intercial regions inside the scans but also these instabilities propogated towards the outside mainly towards the walls of the column. As contrary to the previous studies [10], the interface here in the present study, was not simply comprised of a line having nearly zero thickness. Rather it had a thickness across which

the interfacial fluctuations occurred, this owed to the KH instabilities, which were formed at the interface and subsequently, disseminated into the water with propogating inside it. On the other side, it can alsobe perceived quite well that where the rise in the temperature of the surrounding water helped us to measure the steam water two-phase flows based void fractions, the reduced temperature brings in the descrease in the void fraction, and hence the area under the effect of the interface and steam jet. It also mentioned that the interface has shown a quenching behavior at the lower temperature so the surrounding water temperature could act to stabilize the steam jet inside the water.

4. CONCLUSIONS

The injection of supersonic steam into subcooled water presents a very complex and complicated phenomenon. A sensory system is designed and developed to study this phenomenon and hence the supersonic steam jet indiced direct contact condensation (DCC) phenomena. The system has been developed by using a micro controller, solid state switches and other relating electronic components. Images thus obtained by virtue of the sensors that provide a good evidence of major increment in the diameter of the area under the influence of the supersonic steam jet interface between steam and water. Steam was injected into subcooled water, which has a nearly controlled temperature and the temperature measurements were made with the help of three LM35 digital temperature sensors mounted on the walls of the vessel and PCI-6033 NI DAQ card with 64 analogue channels. It has been observed that with increasing the surrounding water temperature the area under the influence of the interface and hence the steam jet has been raised which has been quantified in terms of the void fraction of the steam jet. Another facet of this problem, which has been addressed in the current study, is the effect of the surrounding water temperature and steam inlet pressure on the hydrodynamic instabilities, which are the main causes of the unstable nature of interface. It has been found that the rise in the surrounding water temperature where helps in the propagation of the steam jet influenced area inside the water, the reduced temperature acts to quinch or reduce the area and hence the propogation and induction of the hydrodynamic instabilities which are the main causes of the turbulent steam jet interface.

REFERENCES

1. Wu X.-Z., Yan J.-J., Li W.-J., Pan D.-D., and Chong, D.-T., *Chem. Eng. Sci.,* 2009, vol. 64, p. 5002. https://doi.org/10.1016/J.CES.2009.08.007

2. Chan, C.K. and Lee, C.K.B., *Int. J. Multiphase Flow,* 1982, vol. 8, p. 11. https://doi.org/10.1016/0301-9322(82)90003-9

3. Kerney, P.J., Faeth, G.M., and Olson, D.R., *AIChE J.,* 1972, vol. 18, p. 548. https://doi.org/10.1002/aic.690180314

4. Weimer, J.C., Faeth, G.M., and Olson, D.R., *AIChE J.,* 1973, vol. 19, p. 552. https://doi.org/10.1002/aic.690190321

5. Del Ttin, G., Lavagno, E., and Malandrone, M., *Proc. 3rd Multi-Phase Flow and Heat Transfer Symposium-Workshop,* Miami Beach, FL, 1983, pp. 134—136.

6. Khan, A., Haq, N.U., Chughtai, I.R., Shah, A., and Sanaullah, K., *Int. J. Heat Mass Transfer,* 2014, vol. 73, p. 521. https://doi.org/10.1016/J.IJHEATMASSTRANSFER.2014.02.035

7. Sanaullah, K., Khan, A., Takriff, M.S., Zen, H., Shah, A., Chughtai, I.R., Jamil, T., Fong, L.S., and Haq, N.U., *Int. J. Heat Mass Transfer,* 2015, vol. 84, p. 178. https://doi.org/10.1016/J.IJHEATMASSTRANSFER.2014.12.073

8. Khan, A., Sanaullah, K., Takriff, M.S., Zen, H., Rigit, A.R.H., Shah, A., Chughtai, I.R., and Jamil, T., *Chem. Eng. Sci.,* 2016, vol. 146, p. 44. https://doi.org/10.1016/J.CES.2016.01.056

9. Datta, D. and Jang, C., *Proc. IAEA 2nd Int. Symposium on Nuclear Power Plant Life Management,* Shanghai, 2007.

10. Shah, A., Chughtai, I.R., and Inayat, M.H., *Chin. J. Chem. Eng.,* 2010, vol. 18, p. 577. https://doi.org/10.1016/S1004-9541(10)60261-3

11. Khan, A., Sanaullah, K., Sobri Takriff, M., Hussain, A., Shah, A., and Rafiq Chughtai, I., *Flow Meas. Instrum.,* 2016, vol. 47, p. 35. https://doi.org/10.1016/J.FLOWMEASINST.2015.12.002

12. Davies, J.T. and Ting, S.T., *Chem. Eng. Sci.,* 1967, vol. 22, p. 1539. https://doi.org/10.1016/0009-2509(67)80192-1

13. Jeffries, R.B., Scott, D.S., and Rhodes, E., *Proc. Inst. Mech. Eng., Conf. Proc.,* 1969, vol. 184, p. 204. https://doi.org/10.1243/pime_conf_1969_184_097_02

14. Van Meulenbroek, B.M. and van de Wakker, B.M., *Int. J. Heat Mass Transfer,* 1985, vol. 28, p. 886. https://doi.org/10.1016/0017-9310(85)90240-6

15. Woodmansee, D.E. and Hanratty, T.J., *Chem. Eng. Sci.,* 1969, vol. 24, p. 299. https://doi.org/10.1016/0009-2509(69)80038-2

16. Wu, X.Z., Yan, J.J., Li, W.J., Pan, D.D., and Chong, D.T., *Chem. Eng. Sci.,* 2009, vol. 64, p. 5002. https://doi.org/10.1016/j.ces.2009.08.007

17. Huang, C.N., Yu, F.M., and Chung, H.Y., *IEEE Trans. Instrum. Meas.,* 2008, vol. 57, p. 1193. https://doi.org/10.1109/TIM.2007.915149

18. Jia, J., Babatunde, A., and Wang, M., *Flow Meas. Instrum.,* 2015, vol. 41, p. 75. https://doi.org/10.1016/j.flowmeasinst.2014.10.010

19. Dyakowski, T., *Meas. Sci. Technol.,* 1996, vol. 7, p. 343. https://doi.org/10.1088/0957-0233/7/3/015

20. Woldesemayat, M.A. and Ghajar, A.J., *Int. J. Multiphase Flow,* 2007, vol. 33, p. 347. https://doi.org/10.1016/j.ijmultiphaseflow.2006.09.004

21. Hanratty, T.J., *Gas-Liquid Flow in Pipelines,* Lemont, IL: Argonne, 2005. https://doi.org/10.2172/837116

22. Zucrow, M.J. and Hoffman, J.D., *Gas Dynamics,* New York: John Wiley & Sons, 1976.

23. *P2000 Electrical Resistance Tomography System ITS System 2000 Version 5.0 Software Operating Manual,* 2005.

24. York, T.A., *Process Imaging for Automatic Control,* Mc-Cann, H. and Scott, D.M., Eds., SPIE, 2001, p. 175. https://doi.org/10.1117/12.417163

25. Pinheiro, P.A.T., Loh, W.W., and Dickin, F.J., *Electron. Lett.,* 1998, vol. 34, p. 69. https://doi.org/10.1049/el:19980092

26. Polydorides, N. and Lionheart, W.R.B., *Meas. Sci. Technol.,* 2002, vol. 13, p. 1871. https://doi.org/10.1088/0957-0233/13/12/310

27. Khan, A., Sanaullah, K., Takriff, M.S., Zen, H., Rigit, A.R.H., Shah, A., Chughtai, I.R., and Jamil, T., *Chem. Eng. Sci.,* 2016, vol. 146, p. 44. https://doi.org/10.1016/j.ces.2016.01.056

28. *Steam Tables, A-to-Z Guide to Thermodynamics, Heat & Mass Transfer, and Fluids Engineering,* New York: Begell House. https://doi.org/10.1615/AtoZ.s.steam_tables

29. Thompson, C.M. and Shure, L., *Image Processing Toolbox: For Use with MATLAB [User's Guide],* Natick, MA: MathWorks, 1995.